

# Equation of state for asymmetric nuclear matter with infinite-order summation of ring diagrams

J. Shamanna\*

*Physics Department, Visva Bharati University, Santiniketan 731235, India*

T.T.S. Kuo

*Physics Department, State University of New York at Stony Brook Stony Brook, NY 11794-3800, USA*

I. Bombaci

*Dipartimento di Fisica, Universita di Pisa, Italy*

Subhankar Ray

*Dept. of Physics, Jadavpur University, Calcutta 700032, India*

(Dated: 18 August 2005)

The particle-particle hole-hole ring-diagram summation method is employed to obtain the equation of state of asymmetric nuclear matter over a wide range of asymmetry fraction. Compared with Brueckner Hartree-Fock and model-space Brueckner Hartree-Fock calculations, this approach gives a softer equation of state, increased symmetry energy and a lower value for the incompressibility modulus which agrees quite well with the values used in the hydrodynamical model for the supernovae explosion.

## 1. INTRODUCTION

A primary aim of microscopic nuclear theories is to derive the various nuclear properties such as the binding energy per nucleon ( $BE/A$ ) and saturation density ( $\rho_0$ ) of nuclear matter, starting from fundamental nucleon-nucleon (NN) interactions. The well-known BHF approach is one such standard nuclear matter theory. In terms of G-matrix diagrams, the BHF theory is, however, only a lowest-order approximation; the ground-state energy shift  $\Delta E_0$  for nuclear matter, due to the NN interaction, is given merely by the first-order G-matrix diagram, fig. 1(a), namely

$$\Delta E_0^{BHF} = \sum_{ab} n_a n_b \langle ab | G^{BHF}(\omega = \epsilon_a + \epsilon_b) | ab \rangle \quad (1)$$

In the above the  $n$ 's are the unperturbed Fermi-Dirac distribution functions,  $n_k=1$  if  $k \leq k_F$  and  $=0$  if  $k > k_F$ .  $k_F$  is the Fermi momentum.

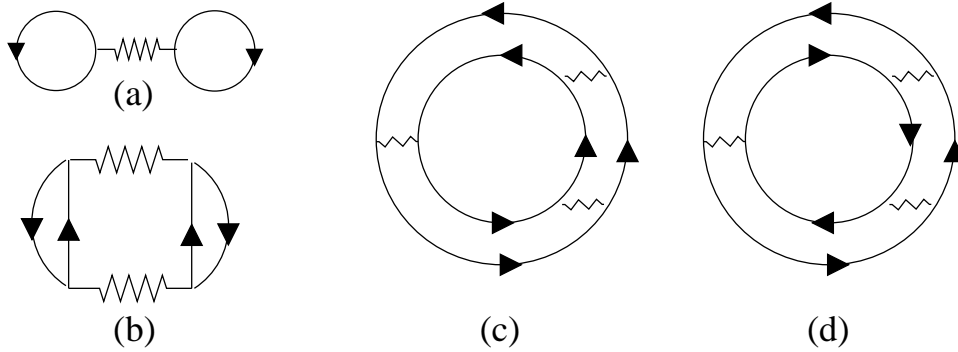


FIG. 1: Some lower order ring diagrams

The single-particle (s.p.) energies denoted by  $\epsilon$ , are determined self-consistently using the BHF theory. As is well known, this approach has not been very successful; it has, in general, not been able to simultaneously reproduce the binding energy per nucleon ( $BE/A = -16 \pm 1$  MeV) and the saturation Fermi momentum ( $k_F^{sat} = 1.35 \pm 0.05$  fm $^{-1}$ ). When plotted on a energy-density plane, results of various BHF calculations for nuclear matter invariably lie, more or less, on a band, the Coester band<sup>1</sup>, which significantly misses the "experimental (empirical) box" for  $BE/A$  and  $k_F^{sat}$ .

The ground state of nuclear matter in BHF theories is treated as merely a Fermi sea. Particle-hole fluctuations near the Fermi sea which represent the long-range correlations are not considered. It should be of interest to allow for such Fermi-sea fluctuations, and they may be important in determining the stiffness of the nuclear-matter equation of state (EOS). Yang, Heyer and Kuo<sup>2</sup> proposed an elegant and rigorous method for summing up particle-particle hole-hole (pphh) and particle-hole (ph) ring diagrams to all orders for the calculation of ground state energies of general many-body system. Inclusion of these classes of diagrams to all orders takes into account the Fermi sea fluctuations and long-range nuclear correlations.

With this motivation, several calculations for symmetric nuclear matter have been carried out with the inclusion of certain class of ring diagrams to all orders<sup>3,4,5</sup>.

In comparison with conventional BHF<sup>6,7</sup> calculations of nuclear matter, the inclusion of the particle-particle hole-hole (pphh) ring diagrams to all orders has the desirable effect of both increasing the nuclear matter binding energy and lowering its saturation density. The final expression for the ground-state energy shift in the pphh ring diagram summation with a model-space reaction G-matrix ( $G^M$ ) is given as

$$\Delta E_0^{ring} = \int_0^1 \frac{d\lambda}{\lambda} \text{tr}\{Y_m(\lambda)Y_m^*(\lambda)G^M(\omega = \Delta_m^{A-2}(\lambda))\lambda\} \quad (2)$$

Comparing with the corresponding BHF result of eq. (1), the main difference between the two methods is the replacement of the unperturbed occupation factors  $n$ , BHF G-matrix  $G^{BHF}$  and starting energy ( $\epsilon_a + \epsilon_b$ ) in the BHF expression by the RPA amplitudes  $Y$ , model-space G-matrix  $G^M$  and RPA energies  $\Delta$ , respectively. In the above  $\lambda$  is a strength parameter introduced to facilitate the calculation, as will be discussed later.

In the present paper, we would like to extend the above ring-diagram scheme to asymmetric nuclear matter, which is in several ways of more physical importance than symmetric (N=Z) nuclear matter. The study of the EOS of asymmetric nuclear matter has become, in the last few years, a subject of renewed interest particularly in connection with astrophysical problems<sup>8,9</sup>, such as supernovae explosions and the evolution of neutron stars. For these physical processes, the nuclear matter involved is predominantly not symmetric, and it is the EOS of asymmetric nuclear matter (with a large neutron excess) which plays an important role for them. Furthermore, the nuclear matter probed by heavy-ion experiments is also generally asymmetric. Here the proton-neutron ratio is about 2/3 for both the target and the projectile, and thus the resulting nuclear matter is likely to be asymmetric with the same proton-neutron ratio. The range of densities sampled by astrophysical systems such as the supernovae and the neutron star vary over an appreciably wide range as do their isospin asymmetries.

According to the model of prompt explosion<sup>10</sup>, which has been widely employed to explain the explosion mechanism of a supernova, the nuclear-matter EOS needs to be relatively soft<sup>8</sup> for the explosion to take place. It should be of interest to investigate the effect of ring diagrams on the stiffness of asymmetric nuclear matter, as we shall carry out later. To our knowledge, such investigations have not yet been performed.

Asymmetric nuclear matter calculations have been done using the Skyrme interactions<sup>11,12</sup>, the Gogny interaction<sup>13</sup> and using the Brueckner-Bethe-Goldstone (BBG) approach<sup>14,15</sup>. Our present calculation is a continuation of the model-space BHF (MBHF) calculations for asymmetric nuclear matter carried out by Song, Wang and Kuo<sup>16</sup>. In the past, the asymmetric nuclear matter properties were often extracted by interpolating the two extreme cases of symmetric and pure neutron matter, with an empirical parabolic approximation<sup>17,18</sup>. The validity of this empirical practice seems to have not been investigated, and we would like to carry out such an investigation by carrying out a sequence of ring-diagram nuclear matter calculations, covering a wide range of proton-neutron ratios and baryon densities.

## 2. FORMALISM

Asymmetric nuclear matter is a system consisting of  $N$  neutrons and  $Z$  protons with  $N \neq Z$ . For symmetric nuclear matter  $N$  and  $Z$  are identical with the same Fermi momenta. For asymmetric matter however, the neutrons and protons are treated as non-identical particles with different Fermi momenta.

We introduce a parameter  $\alpha$  as a measure of the asymmetry in nuclear matter, namely

$$\alpha = \frac{(\rho_n - \rho_p)}{\rho} = \frac{(N - Z)}{A} \quad (3)$$

where  $\rho$ ,  $\rho_n$  and  $\rho_p$  are respectively the nuclear, the neutron and the proton densities. The neutron and the proton Fermi momentum are

$$k_F^n = (3\pi^2 \rho_n)^{1/3} \quad k_F^p = (3\pi^2 \rho_p)^{1/3} \quad (4)$$

An average Fermi momentum is defined as

$$k_F = \left(\frac{3}{2}\pi^2\rho\right)^{1/3} \quad (5)$$

### 3. MODEL-SPACE G-MATRIX AND SINGLE-PARTICLE SPECTRUM

As with the symmetric case we start with a Hamiltonian  $H = T + V$ . Introducing a single particle (s. p.) potential  $U$  we rewrite it as  $H = (T + U) + (V - U)$ .  $V$  is the NN potential such as the Paris<sup>19</sup> or the Bonn<sup>20</sup> potential. A model space  $P$  is defined as a configuration space where all nucleons are restricted to have the momentum  $k \leq k_M$ ,  $k_M$  being the momentum space boundary of  $P$ . A typical value for  $k_M$  is  $2k_F$  where  $k_F$  is the Fermi momentum. As we shall discuss later, most of the calculations in the present work are performed using  $k_M=3.0 \text{ fm}^{-1}$ .

Similar to the case of symmetric nuclear matter we use a model-space Hartree-Fock method<sup>21,22,23</sup> to determine  $U$ . This leads to the following self-consistent equations for the s.p. spectrum  $\epsilon_i^M$ , namely

$$\epsilon_i^M = t_{k_i} + \Gamma_{k_i}(k_i, \tau_i) \quad (6)$$

$$\Gamma_{k_i}(\omega, \tau_i) = 2 \sum_{\substack{\tau_j, s_i, s_j \\ k_j \leq k_F^{\tau_j}}} \langle k_i k_j | G^M(\omega + \epsilon_j) | k_i k_j \rangle \quad k_i \leq k_M \quad (7)$$

$$\Gamma_{k_i}(\omega, \tau_i) = 0 \quad k_i > k_M \quad (8)$$

Note that the subscript  $i$  represents both momentum and isospin, namely  $i \equiv (\mathbf{k}_i, \tau_i)$  with  $\mathbf{k}_i$  denoting the momentum and  $\tau_i$  the  $z$  component of the isospin of the  $i$ th nucleon. The single particle kinetic energy is  $t_{k_i} = \hbar^2 k_i^2 / 2m$ ,  $G^M$  is the reaction matrix to be specified later. The Fermi momentum is represented by  $k_F^{\tau_j}$  with neutron Fermi momentum  $k_F^n$  for  $\tau_j = -\frac{1}{2}$ , and proton Fermi momentum  $k_F^p$  for  $\tau_j = \frac{1}{2}$ . The model-space momentum boundary is  $k_M$  and is taken to be the same for neutrons and protons. The s.p. potential is the one-body vertex function  $\Gamma$  evaluated at the self-consistent energy  $\omega = \epsilon_{k_i}$

$$U(k_i, \tau_i) = \Gamma_{k_i}(\epsilon_{k_i}, \tau_i), \quad i \equiv n, p \quad (9)$$

$U(k_i, \tau_i)$  is determined self-consistently for  $k_i \leq k_M$ , and for  $k_i > k_M$  we set  $U = 0$ . We also use an effective mass description for the single particle spectrum as

$$\epsilon_{k_i}^M = \begin{cases} (\hbar^2/2m_q^*)k_i^2 + \Delta_q, & k_i \leq k_M \\ (\hbar^2/2m)k_i^2, & k_i > k_M \end{cases} \quad (10)$$

with four parameters  $m_q^*, \Delta_q$ , ( $q = n, p$ ). The effective mass  $m^*$  and the zero point energy  $\Delta$  are determined self-consistently.

The model-space reaction matrix  $G^M$  satisfies the Bethe-Goldstone equation

$$\langle ij | G^M(\omega) | mn \rangle = \langle ij | V | mn \rangle + \sum_{k,l} \frac{\langle ij | V | kl \rangle Q^M(k, l) \langle kl | G^M(\omega) | mn \rangle}{\omega - \epsilon_k - \epsilon_l} \quad (11)$$

In the above equation  $i, j, m, n, k$  and  $l$  are single particle states, each with momentum  $\mathbf{k}$ , isospin  $\tau$ .  $V$  is the nucleon-nucleon interaction. The energy variable  $\omega$  in the denominator of eq. (11) is given by

$$\omega = \epsilon_k^M + \epsilon_l^M \quad (12)$$

The two particle correlations considered are those where at least one particle is out of the model space. Hence the Pauli operator  $Q^M$  is defined as

$$Q^M(k, l) = \begin{cases} 1, & \text{if } \max(k_k, k_l) > k_M \text{ and } k_k > k_F^{\tau_k}, k_l > k_F^{\tau_l} \\ 0, & \text{otherwise} \end{cases} \quad (13)$$

Note that  $Q^M$  is different for each of the following three cases of the intermediate two nucleon state.

For the  $nn$  ( $pp$ ) case (fig.2(a)), the intermediate nucleons are identical, and only  $k_M$  and  $k_F^q$ ,  $q = n$  or  $p$ , enter the calculation. For the  $np$  or  $pn$  case however,  $k_M$ ,  $k_F^n$  and  $k_F^p$  all play a role in determining  $Q^M$  (fig.2(b)). It is

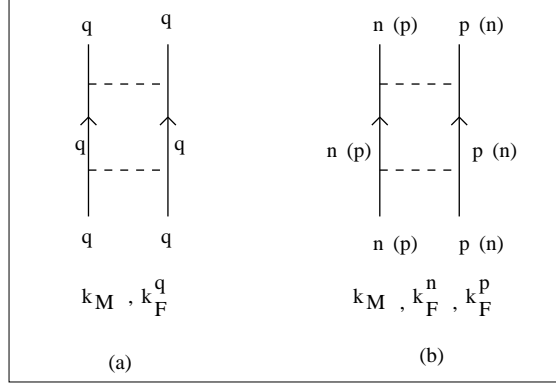


FIG. 2: Intermediate two nucleon states in the asymmetric case (a)  $nn$  or  $pp$  (b)  $np$  or  $pn$ .

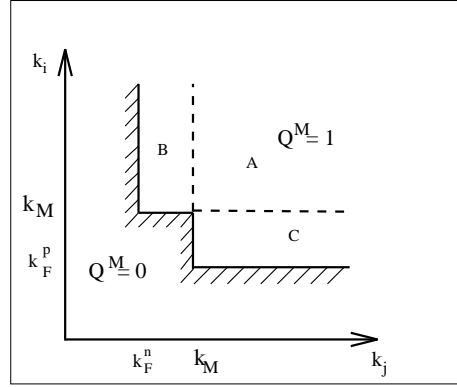


FIG. 3: Pauli operator  $Q^M(k_k, k_l)$

convenient to carry out the above calculation in the relative and center of mass (RCM) frame. We choose our relative momentum  $\mathbf{k}$  and center of mass momentum  $\mathbf{K}$  as

$$\mathbf{k} = \frac{1}{2}(\mathbf{k}_k - \mathbf{k}_l), \quad \mathbf{K} = (\mathbf{k}_k + \mathbf{k}_l) \quad (14)$$

First we replace the Pauli exclusion operator  $Q^M$ , which is a function of the laboratory momenta by its angle average approximation  $\bar{Q}^M$ . We divide the plane of the two laboratory momenta into three regions A, B and C as shown in fig.3. The values of  $Q^M$  in the three regions are shown in the figure. Each of the regions is transformed into the RCM frame. Then the angle-averaged value of  $Q^M$  is

$$\bar{Q}^M = \bar{Q}_A^M + \bar{Q}_B^M + \bar{Q}_C^M \quad (15)$$

where, for region B, we have

$$\bar{Q}_B^M(k, K) = \begin{cases} 0 & \text{regions } a, b \\ ((k + \frac{1}{4}K)^2 - k_M^2)/2kK & \text{region } c \\ (k_M^2 - (k - \frac{1}{2}K)^2)/2kK & \text{region } d \\ (2k^2 + \frac{1}{2}K^2 - k_M^2 - (k_F^n)^2)/2kK & \text{region } e \\ (k_M^2 - (k_F^n)^2)/2kK & \text{region } f \end{cases} \quad (16)$$

The subdomains a to e are shown in fig.4 and  $2(k_C^n)^2 = [(k_F^n)^2 + k_M^2]$ . Angle average approximations are standard (and indispensable) in treating Pauli exclusion operators in nuclea matter calculations and are generally considered to be accurate<sup>24,25</sup>. This technique has the advantage of making the model-space reaction matrix diagonal in the RCM variables. Recent studies of an exact pauli operator calculation have been reported<sup>26</sup>. It is not very clear whether such calculations show an appreciable difference in the binding energy per nucleon and the saturation density from previous studies. Angle averages for region C may be obtained from the above by substituting  $k_F^p$  for  $k_F^n$ . The calculation

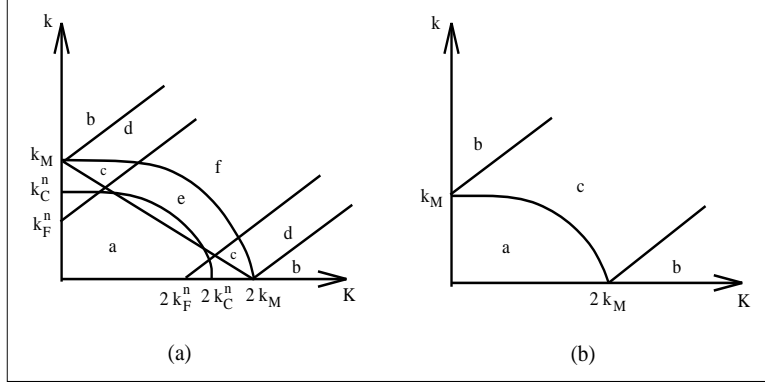


FIG. 4: Angle averaged Pauli operator  $\bar{Q}_B^M$  and  $\bar{Q}_A^M$ .

above was an illustration of the case where the intermediate state contains one neutron and one proton. The other two possibilities may be readily obtained from fig.3 above by suitable substitution of the relevant Fermi momentum.

A similar RCM mapping of region A in fig.3 gives

$$\bar{Q}_A^M(k, K) = \begin{cases} 0 & \text{region a} \\ 1 & \text{region b} \\ (k^2 + \frac{1}{4}K^2 - k_M^2)/kK & \text{region c} \end{cases} \quad (17)$$

For symmetric nuclear matter  $k_F^n = k_F^p$  so that  $\bar{Q}_B^M = \bar{Q}_C^M$  and the angle averaged  $Q^M$  is the same as that given in eq. (16)

Using the angle averaged Pauli operator the model space reaction matrix can be decomposed into separate partial wave channels as

$$\langle kl|G^M(\omega, Kw)|k'l'\rangle = \langle kl|V|k'l'\rangle + \frac{2}{\pi} \int_0^\infty dk'' k''^2 \sum_{l''} \frac{\langle kl|V|k''l''\rangle \bar{Q}^M(k'', K) \langle k''l''|G^M(\omega, Kw)|k'l'\rangle}{\omega - H_0(k'', K)} \quad (18)$$

where  $w$  denotes the partial wave quantum numbers ( $l'SJT$ ), and  $K$  is the center of mass momentum. The  $K$  and ( $SJT$ ) quantum numbers associated with the bra and ket vectors have been suppressed for simplicity. For example,  $\langle kl|$  should in fact be  $\langle klSJT, K|$ . Our convention for plane waves is

$$\langle \mathbf{r}|klSJ\rangle = j_l(kr) \mathcal{Y}_{lSJ}(\hat{\mathbf{r}}) \quad (19)$$

where  $j_l(kr)$  is the spherical Bessel function, and  $\mathcal{Y}$  is the vector spherical harmonics corresponding to  $\mathbf{l}=\mathbf{S}+\mathbf{J}$ . The angle averaged reaction matrix  $G^M(\omega, Kw)$  is diagonal in  $K$  and  $w$ . This is a consequence of using angle averages for the projection operator  $Q^M$  and the energy denominator.

From eq. (12) the energy variable in the laboratory frame is  $\epsilon_i + \epsilon_h$ . Using RCM variables, the energy denominator  $\omega$  for the neutron spectrum is given by

$$\omega = \frac{\hbar^2}{m_p^*} k^2 + \frac{\hbar^2}{4m_p^*} K^2 + \Delta_n + \Delta_p + \left[ \frac{\hbar^2}{2m_n^*} - \frac{\hbar^2}{2m_p^*} \right] (k^n)^2 \quad (20)$$

Similar expression is obtained for the proton spectrum by replacing the subscripts and superscript  $n$  by  $p$ . The other term in the denominator  $H_0 = \epsilon_m + \epsilon_n$  is the unperturbed energy of the intermediate states and is also angle dependent. The momentum variables  $k_m$  and  $k_n$  corresponding to  $k$  and  $K$  may be in either of the three regions A, B or C. In region A, both intermediate particles have momentum larger than  $k_M$ . Therefore we have

$$H_0^A(k, K) = \frac{\hbar^2}{m} k^2 + \frac{\hbar^2}{4m} K^2 \quad (21)$$

In region B, we have a proton with momentum larger than  $k_M$  and a neutron with momentum between  $k_F^n$  and  $k_M$ . We use an angle average approximation for  $k_m^2$  i.e.,  $\langle k_m^2 \rangle = \frac{1}{2}[(k_F^n)^2 + k_M^2]$  and obtain

$$H_0^B(k, K) = \frac{\hbar^2}{m} k^2 + \frac{\hbar^2}{4m} K^2 + \Delta_n + \frac{\hbar^2}{4m} \left[ \frac{m}{m_n^*} - 1 \right] [(k_F^n)^2 + k_M^2] \quad (22)$$

The spectrum of  $H_0$  for region C is the same as that of region B with the subscripts and superscript  $n$  changed to  $p$ . Finally the single particle potential in the (RCM) frame for  $k_1 \leq k_F^{\tau_q}$  with ( $q \equiv n, p$ ) is given as

$$U(k_1, \tau_q) = \frac{16}{\pi} \sum_{lSJ\tau_j} (2J+1) \int_0^{k_-} dk k^2 G_{lSJ\tau_q\tau_j}^M(k, \bar{K}_1) + \frac{2}{\pi k_1} \sum_{lSJ\tau_j} (2J+1) \int_{k_-}^{k_+} dk k [(k_F^{\tau_j})^2 - k_1^2 + 4k(k_1 - k)] G_{lSJ\tau_q\tau_j}^M(k, \bar{K}_2) \quad (23)$$

And for  $k_1 > k_F^{\tau_q}$  but less than  $k_M$  we have

$$U(k_1, \tau_q) = \frac{2}{\pi k_1} \sum_{lSJ\tau_j} (2J+1) \int_{k_-}^{k_+} dk k [(k_F^{\tau_j})^2 - k_1^2 + 4k(k_1 - k)] G_{lSJ\tau_q\tau_j}^M(k, \bar{K}_2) \quad (24)$$

where

$$\begin{aligned} k_- &= \frac{1}{2} |k_F^{\tau_j} - k_1| \\ k_+ &= \frac{1}{2} (k_F^{\tau_j} + k_1) \\ \bar{K}_1^2 &= 4(k_1^2 + k^2) \\ \bar{K}_2^2 &= 4(k_1^2 + k^2) - (2k + k_1 - k_F^{\tau_j})(2k + k_1 + k_F^{\tau_j}) \end{aligned} \quad (25)$$

and the partial wave reaction matrix elements are given by

$$G_{lSJ\tau_i\tau_j}^M(k, K) = \langle kl\tau_i\tau_j | G^M(\omega, KlSJ) | kl\tau_i\tau_j \rangle \quad (26)$$

Eq. (18) is in isospin representation with well defined total isospin  $T$  of the two nucleon state. The reaction matrix elements in the neutron-proton representation i.e., eq. (26), are related to those in the isospin representation by Clebsch-Gordon coefficients; which explains the factor of 2 in the expression for the s.p. potential.

The s.p. potentials  $U(k_1, \tau_n)$ ,  $U(k_1, \tau_p)$  and the spectra  $\epsilon_n$ ,  $\epsilon_p$  are calculated self-consistently as described previously. A main purpose here is to convert the strong  $V$  interaction to a well-behaved G-matrix interaction. In so doing, one must make sure that there is no double counting. Thus a double-partitioned approach is adopted, treating the nucleon-nucleon correlations with high momentum (i.e. those with  $Q^M = 1$ ) within the  $G^M$  matrix, while taking care of the low-momentum correlations by the pphh ring diagrams. We would like to express the energy shift in terms of the model space G-matrix<sup>3</sup>.

Proceeding as in Ref. (3) we define a model-space G-matrix and formulate an expression for the energy shift in terms of the transition amplitudes as

$$\Delta E_0^{pp} = \int_0^1 \frac{d\lambda}{\lambda} \sum_{(A-2)}^m \sum_{\substack{i>j, k>l \\ \in P}} Y_m(ij, \lambda) Y_m^*(kl, \lambda) G_{kl ij}^M([\omega = \Delta_m^{A-2}(\omega)]) \lambda \quad (27)$$

with

$$\begin{aligned} \sum_{e>f} \{\delta_{ij,ef}(\varepsilon_i + \varepsilon_j) + (1 - n_i - n_j)\lambda L_{ijef}(\omega)\} Y_m(ef, \lambda) &= \Delta_m^{A-2}(\omega) Y_m(ij, \lambda) \\ \omega &= \Delta_m^{A-2}(\omega) \end{aligned} \quad (28)$$

For the neutron-neutron ( $nn$ ) or the proton-proton ( $pp$ ) cases, the inequality signs for the summation indices  $i, j, k, l$  restrict the momentum  $k_i \geq k_j$ , similarly for  $k_k$  and  $k_l$  to avoid double counting. The neutron-proton ( $np$ ) or the proton-neutron ( $pn$ ) case is more complicated. Here a free summation over the indices gives four terms with identical contribution (two for each of  $np$  and  $pn$  cases) and a factor of (1/2) would be needed for correct counting. Thus in our calculation for this case we have confined the indices  $i, k, e$  to neutrons and  $j, l, f$  to protons with their momentum summations unrestricted.

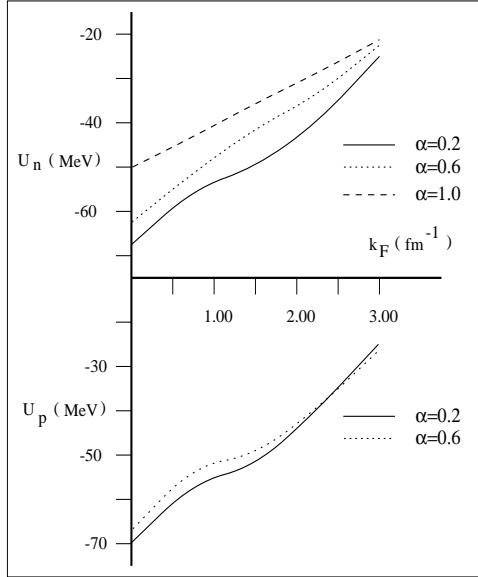


FIG. 5: Neutron ( $U_n$ ) and proton ( $U_p$ ) s.p. potentials.

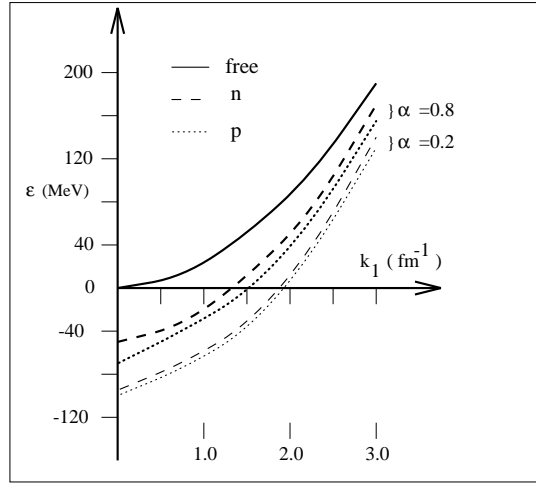


FIG. 6: Single particle spectra for neutron and proton calculated with the model space approach at  $\alpha = 0.2$  and  $0.8$  for  $k_F = 1.35 \text{ fm}^{-1}$  with Paris interaction.

#### 4. RESULTS OF THE S.P. SPECTRUM CALCULATION

Fig.(5) shows the neutron (upper part) and the proton (lower part) s.p. potentials for different  $\alpha$ . As the proton fraction decreases the s.p. potentials become less deep and  $U_p$  vanishes when the proton fraction becomes zero.

For the asymmetric case as well, the spectrum is continuous from momentum 0 to  $k_M$  as shown in fig.6, unlike the usual BHF spectrum which has a large discontinuity at  $k_F$ . Beyond  $k_M$  we use a free s.p. spectrum since our method is designed for determination of the s.p. spectrum within the model space only. Our spectrum has a small discontinuity of around 4 – 5 MeV at  $k_M$ .

Table 1 lists the  $m/m^*$  values and zero point energies at  $\alpha = 0.2$  and  $\alpha = 0.8$  for various average Fermi momentum at a model space boundary of  $3.0 \text{ fm}^{-1}$ . With increase in  $\alpha$ ,  $\Delta_n$  increases and  $\Delta_p$  decreases for small  $k_F$ . For the same asymmetry fraction, both  $\Delta_n$  and  $\Delta_p$  become deeper with increase in  $k_F$ . The change in the effective mass with the asymmetry fraction is very small though for the same asymmetry fraction it increases with  $k_F$ . For  $\alpha = 0.0$ , the s.p. potential, the effective masses and the zero point energies match the ones calculated previously for the symmetric case which also serves as a test for the reliability of our asymmetric matter calculation. The calculated binding energy for a given combination of the asymmetry parameter  $\alpha$  and the Fermi momentum  $k_F$  depends on the model-space

TABLE 1: Typical  $m^*$  and  $\Delta$  values calculated with the Paris NN interaction at  $\alpha = 0.2$  and  $0.8$ .

	$k_F$ (fm $^{-1}$ )	$m/m_n^*$	$\Delta_n$ (MeV)	$m/m_p^*$	$\Delta_p$ (MeV)
$\alpha = 0.2$	1.00	1.10	-29.44	1.10	-31.45
	1.20	1.15	-46.61	1.16	-48.89
	1.35	1.21	-61.69	1.21	-63.73
	1.50	1.26	-77.38	1.26	-76.83
	1.70	1.34	-96.75	1.34	-97.13
$\alpha = 0.8$	1.00	1.08	-24.66	1.10	-33.05
	1.20	1.13	-40.05	1.15	-49.56
	1.35	1.17	-52.16	1.19	-60.60
	1.50	1.23	-66.47	1.24	-74.05
	1.70	1.32	-86.55	1.32	-91.68

size. On minimizing the energy against the model-space momentum, Song, Wang and Kuo<sup>16</sup> found for their MBHF calculations that for each combination of  $\alpha$  and  $k_F$  there was one value of  $k_M$  for which the energy was a minimum. For the same  $\alpha$ , the energy minimum shifted towards smaller values of  $k_M$ . For values of  $k_F$  ranging between 0.50 to 1.80 the minimum values of  $k_M$  were between 2.80 to 3.4. Based on this we have made our choice of  $k_M$  to be 3.0 fm $^{-1}$ .

## 5. THE RPA EQUATION

Let us recall our RPA-type secular equation

$$\sum_{e>f} \{(\epsilon_i + \epsilon_j)\delta_{ij,ef} + (\bar{n}_i\bar{n}_j - n_in_j)\lambda L_{ijef}(\omega)\} Y_m(ef, \lambda) = \mu_m(\omega, \lambda) Y_m(ij, \lambda) \quad (29)$$

with the self consistent condition

$$\begin{aligned} \mu_m(\omega, \lambda) &= \omega \equiv \omega_m^-(\lambda) \\ L_{ijef}(\omega) &\equiv \bar{G}_{ijef}^M(\omega) \end{aligned} \quad (30)$$

The above RPA-type equation is in laboratory momentum variables. As for the symmetric case, we transform the above equation into its RCM representation. We also do an angle average for the occupation factor  $(\bar{n}_i\bar{n}_j - n_in_j) = 1 - (n_i + n_j)$ . We define a function  $Q_R(k_i, k_j) = 1 - (n_i + n_j)$ . It is equal to +1 or -1 depending on the values of  $k_i$  and  $k_j$ .  $Q_R$  is +1 in regions A and B ( $i, j$  both are particles); is -1 in region C ( $i, j$  are both holes) and is equal to zero for all other regions. The value of  $Q_R$  depends on the angle between  $\mathbf{k}$  and  $\mathbf{K}$ . Let us denote by  $\tau_z$  the  $z$ -component of the total isospin  $T$  of the two nucleon state i.e.,  $\tau_z = \tau_i + \tau_j$ . As the two nucleon state can be either  $nn$ ,  $pp$  or  $np$  ( $pn$ ),  $\tau_z$  can take the values -1, 1 or 0. For the case when  $\tau_z = +1$  or  $-1$  the two nucleons are identical and the situation is no different from the symmetric case ( $\bar{Q}_R$  is the same as eq. (4.9) in Ref. (3). For  $\tau_z = 0$  we obtain the angle averaged  $\bar{Q}_R$  as

$$\bar{Q}_R(k, K) = \begin{cases} -1 & \text{region 1} \\ -|x_1| & 2 \\ 1 & 3 \\ |x_1| & 4 \\ |x_2| & 5 \\ \min(|x_1|, |x_2|) & 6 \end{cases} \quad (31)$$

where

$$\begin{aligned} k_a &= \frac{k_F^n + k_F^p}{2} \\ x_1 &= \frac{k^2 + \frac{1}{4}K^2 - k_a^2}{kK} \\ x_2 &= \frac{k_M^2 - k^2 - \frac{1}{4}K^2}{kK} \end{aligned}$$



The above angle averages are obtained under the assumption that all values for the angle between  $\mathbf{k}$  and  $\mathbf{K}$  are equally likely. The regions 1 to 6 refer to the regions in the  $(k, K)$  plane as shown in the figure. The replacement of the

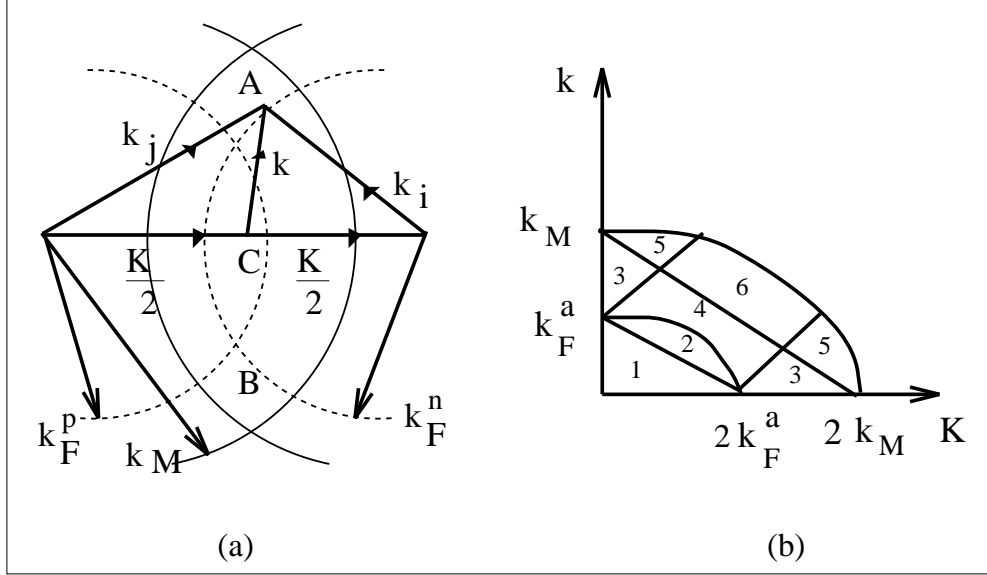


FIG. 7: Angle average of occupation factor  $Q_R(k_i, k_j)$

occupation factor  $Q_R$  by its angle-averaged quantity greatly simplifies the RPA-type secular equation we started with. Now it can be decomposed into separate partial wave channels

$$\begin{aligned} & \sum_{l'} \int dk' \{ \epsilon_{kK} \delta(k - k') \delta_{ll'} + \lambda \frac{2k'^2}{\pi} \bar{Q}_R(k, K) \langle kl | L(\omega, K) | k'l' \rangle \} Y_m(k'l'k, \lambda) \\ & = \mu_m(\omega, \lambda) Y_m(klK, \lambda) \end{aligned} \quad (32)$$

where  $\bar{Q}_R(k, K)$  is actually  $\bar{Q}_R(k, K, k_F^{\tau_i}, k_F^{\tau_j}, k_M)$ .  $\epsilon_{kK}$  is the unperturbed energy. There is a subtle point. For the  $nn$  or  $pp$  cases where the two nucleons are identical this unperturbed energy may be taken simply as  $\frac{\hbar^2}{m} k^2 + \frac{\hbar^2}{4m} K^2 + 2U(\bar{k}_1, \tau_q)$ , where  $\bar{k}_1^2 = (k^2 + \frac{1}{4}K^2)$  is the angle averaged value for the momenta of the two nucleons and  $q = n$  or  $p$ . For the  $np$  ( $pn$ ) case, this averaging is more complicated. One way around this is in the choice of relative  $k$  mesh points. For each  $K$  mesh point we choose the  $k$  such that the RCM values of  $k_n$  and  $k_p$  are either both in the hole region or both in the particle region. With such a choice of mesh points the sum of the squares of the individual neutron and proton momenta in the RCM frame, both being either holes or particles is  $\bar{k}_n^2 + \bar{k}_p^2 = (k^2 + \frac{1}{4}K^2)$ . Hence the value of the unperturbed energy is

$$\frac{\hbar^2}{m} k^2 + \frac{\hbar^2}{4m} K^2 + U(\bar{k}_1, \tau_n) + U(\bar{k}_1, \tau_p)$$

with  $\bar{k}_1^2 = (k^2 + \frac{1}{4}K^2)/2$ .

The wave function  $(kl)$  denotes the RCM partial wave function  $(klSJT_1T_2, K)$  and similarly for  $(k'l')$ . The above equation is to be solved together with the self consistent condition  $\mu_m(\omega, \lambda) = \omega_m^-(\lambda)$  giving the self-consistent solution  $\omega_m^-(\lambda)$ .

The vertex function  $L(\omega, \tau_1\tau_2, K)$  in the above equation is the irreducible vertex function which has both one-body and two-body G-matrix diagrams<sup>3</sup>. These contribute significantly to the depletion of s. p. orbits below  $k_F$ , especially at high density. As we are working in the RCM frame an angle average approximation is employed to obtain  $L$  in the RCM frame for the  $\tau_z = 0$  case as

$$\begin{aligned} \langle kl | L(\omega, \tau_n\tau_p, K) | k'l' \rangle & = \langle kl\tau_n\tau_p | \bar{G}^M(\omega, Kw) | k'l'\tau_n\tau_p \rangle \\ & + \delta_{kk'} \delta_{ll'} \{ \Gamma_{\bar{k}_n}(\omega - \epsilon_{\bar{k}_p}, \tau_n) - U(\bar{k}_n, \tau_n) \\ & + \Gamma_{\bar{k}_p}(\omega - \epsilon_{\bar{k}_n}, \tau_p) - U(\bar{k}_p, \tau_p) \} \end{aligned} \quad (33)$$

where

$$\begin{aligned}
\bar{k}_n^2 &= \bar{k}_p^2 = (k^2 + \frac{1}{4}K^2)/2 \\
\epsilon_{\bar{k}_n} &= \frac{\bar{k}_n^2}{2m} + U(\bar{k}_n, \tau_n) \\
\epsilon_{\bar{k}_p} &= \frac{\bar{k}_p^2}{2m} + U(\bar{k}_p, \tau_p)
\end{aligned} \tag{34}$$

The other two cases for  $\tau_z = -1$  or  $1$  can be obtained by suitable substitution of  $\tau_p$  and  $\tau_n$ .

## 6. RESULTS AND DISCUSSIONS

### 6.1. Binding energy

The energy shift is given as

$$\begin{aligned}
\frac{\Delta E_0^{pp}}{A} &= \frac{6}{\pi^2[(k_F^n)^3 + (k_F^p)^3]} \sum_w \sum_{\tau_z} (2J+1) \int_0^1 d\lambda \int_0^{2k_F^{\tau_z}} dK K^2 \\
&\times \sum_{mll'} \int_0^{k_M} dk k^2 \int_0^{k_M} dk' k'^2 Y_m^*(klK, \lambda) \times \langle kl\tau_1\tau_2 | G^M(\omega, Kw) | k'l'\tau_1\tau_2 \rangle Y_m(k'l'K, \lambda)
\end{aligned} \tag{35}$$

where  $\tau_z = -1, 0, 1$  for  $T = 1$  and  $\tau_z = 0$  for  $T = 0$  and

$$k_F^{\tau_z} = \begin{cases} k_F^n & \text{for } \tau_z = -1 \\ (k_F^n + k_F^p)/2 & \text{for } \tau_z = 0 \\ k_F^p & \text{for } \tau_z = 1 \end{cases} \tag{36}$$

The binding energy per nucleon is given as

$$\frac{-BE}{A} = \frac{3\hbar^2}{20m} [(1+\alpha)(k_F^n)^2 + (1-\alpha)(k_F^p)^2] + \frac{\Delta E_0^{pp}}{A} \tag{37}$$

We present the results of our ring calculation in table 2 and in figs.8 and 9 using Paris NN interactions, for various

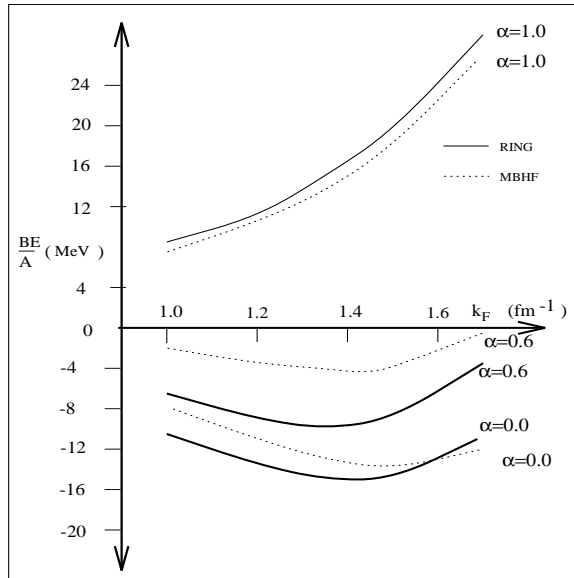


FIG. 8:  $BE/A$  from Ring diagram summation at three asymmetry values :  $\alpha = 0.0, 0.6$  and  $1.0$

values of the Fermi momentum and the asymmetry fraction. The binding energy at  $\alpha = 0.0$  (symmetric nuclear

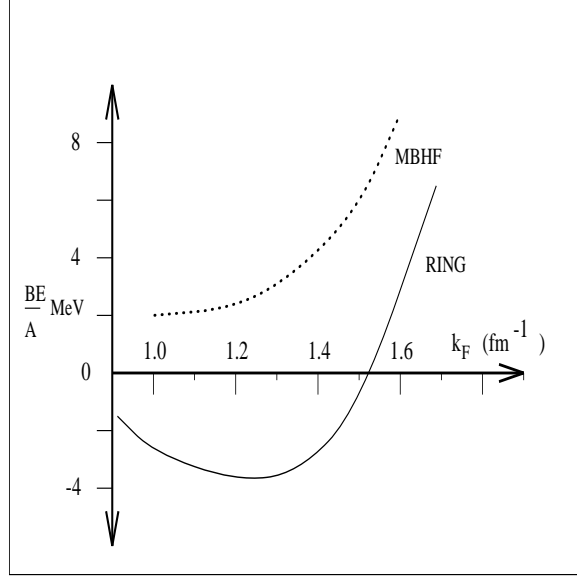


FIG. 9:  $BE/A$  versus  $k_F$  with Ring summation and MBHF calculation at  $\alpha = 0.8$ . The ring curve shows a saturation which is not present in the MBHF curve.

TABLE 2:  $BE/A$  in MeV for various combinations of  $\alpha$  and  $k_F$  ( $\text{fm}^{-1}$ ) with  $k_M = 3.0$  ( $\text{fm}^{-1}$ ) and Paris interaction. Results from (MBHF) calculation are also given for comparison.

$\alpha/k_F$	0.65	1.00	1.20	1.35	1.50	1.70
0.0	-6.26 (-3.74)	-10.89 (-8.60)	-14.02 (-11.40)	-15.68 (-13.31)	-15.66 (-14.43)	-12.76 (-13.47)
0.2	-5.87 (-3.42)	-10.49 (-7.94)	-13.47 (-10.56)	-14.97 (-12.38)	-15.00 (-13.27)	-11.64 (-12.12)
0.4	-5.78 (-2.44)	-9.60 (-5.99)	-12.32 (-8.00)	-13.30 (-9.32)	-12.76 (-9.60)	-8.58 (-7.76)
0.6	-5.18 (-0.91)	-7.42 (-2.68)	-9.62 (-3.65)	-10.04 (-4.02)	-8.87 (-3.30)	-2.40 (-0.03)
0.8	-1.90 (1.29)	-3.52 (2.00)	-3.83 (2.51)	-3.54 (3.52)	-1.11 (5.70)	6.40 (11.00)
1.0	4.03 (4.08)	8.11 (8.07)	11.03 (10.84)	14.22 (13.74)	19.02 (17.85)	29.65 (26.20)

matter) by our ring calculation is -15.93 MeV which is good agreement with the empirical value. The saturation Fermi momentum is  $1.43 \text{ fm}^{-1}$ . As the asymmetry fraction increases ( the proton fraction decreases), both the binding energy and the saturation Fermi momentum drop till at  $\alpha = 1.0$  (zero proton fraction) there is no saturation. An interesting result of the ring calculation is the existence of saturation at  $\alpha = 0.8$  which is not present in the MBHF calculation.

TABLE 3:  $E_{sym}^{Ring}$  calculated from eq. (38) and eq. (39) and  $E_{sym}^{MBHF}$ .

$k_F (fm^{-1})$	$E_{sym}^{Ring}$	$E_{sym}^{MBHF}$	Empirical
0.65	9.84	8.17	10.29
1.00	18.48	16.07	19.00
1.20	23.81	21.23	25.05
1.35	28.29	25.42	29.90
1.50	32.79	29.72	34.68
1.70	40.53	35.61	42.41

## 6.2. Symmetry energy

The symmetry energy is defined as

$$E_{sym}^{Ring}(k_F) = \frac{1}{2} \left. \frac{\partial^2 W(\alpha, k_F)}{\partial \alpha^2} \right|_{\alpha=0} \quad (38)$$

where  $W(\alpha, k_F)$  is the binding energy at a given  $\alpha$  and  $k_F$ . To ascertain the nature of the dependence of the binding energy on the asymmetry parameter we have tried fitting a polynomial curve of leading order  $\alpha^2$  and higher for the residuals upto to the order of  $\alpha^6$  to our data. Using eq. (38) and the parameters of the above fit we obtain the  $E_{sym}^{Ring}$  for various values of  $k_F$  as shown in table 3. The corresponding values obtained by the MBHF calculation<sup>16</sup> are also shown for comparison. The value of the symmetry energy calculated by our method is consistently higher than the corresponding MBHF calculations as is shown by fig.10. Thus the ring diagram summation improves the symmetry energy values as well. At the saturation density ( $\rho_0 = 0.17 \text{ fm}^{-3}$ )  $E_{sym}^{Ring}$  is 28 MeV which is close to the value of 31 MeV reported in an independent calculation<sup>27</sup>. Empirically,  $E_{sym}^{Ring}$  may be simply evaluated from the two extreme cases of pure neutron matter and symmetric nuclear matter shown in the fourth column of table 3.

$$E_{sym}(k_F) = W(1, k_F) - W(0, k_F) \quad (39)$$

The  $E_{sym}$  calculated with eq. (38) and eq. (39) differ by about .5 MeV to 1.8 MeV .

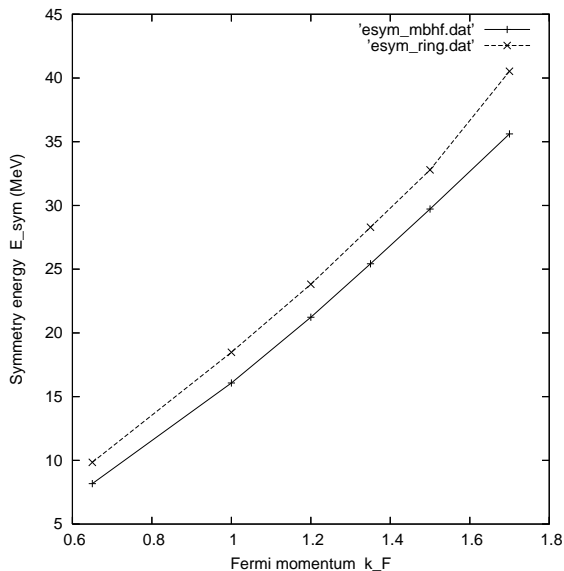


FIG. 10: Symmetry energy obtained from Ring (upper curve) and MBHF (lower curve) calculations.

TABLE 4:  $\kappa_0(\alpha)$  calculated from eq. (40).

$\alpha$	$k_F^{sat}(fm^{-1})$	$\kappa_0(\alpha)$	$W_0(\alpha)$
0.0	1.43	114.51	-15.93
0.2	1.43	100.20	-15.25
0.4	1.39	92.74	-13.33
0.6	1.33	67.35	-10.05
0.8	1.24	22.95	-3.85

### 6.3. Incompressibility

In describing the iron-core collapse of a presupernova using hydrodynamical models, the basic physical inputs are the initial mass of the core and the nuclear EOS. The EOS of asymmetric nuclear matter exhibits a minimum which disappears before pure neutron matter is reached. Therefore we expect that the incompressibility modulus decreases with respect to the symmetric case and vanishes before the proton fraction vanishes. The incompressibility modulus is defined as

$$\kappa_0(\alpha) = k_{F_0}^2(\alpha) \left. \frac{d^2 W(\alpha, k_F)}{dk_F^2} \right|_{k_F=k_{F_0}(\alpha)} \quad (40)$$

where  $k_{F_0}(\alpha)$  is the saturation Fermi momentum at the given  $\alpha$ . One of the most sophisticated investigation of the  $\alpha$  dependence of  $\kappa_0$  and  $\rho_0$  so far has been done in Ref. (14) in the framework of BBG (Brueckner-Bethe- Goldstone) theory. They found that for low  $\alpha$  values ( $\alpha \leq 0.4$ )  $\kappa_0$  and  $\rho_0$  show a parabolic dependence on  $\alpha$

$$\kappa_0(\alpha) = \kappa_0(0)(1 - a \alpha^2) \quad (41)$$

$$\rho_0(\alpha) = \rho_0(0)(1 - b \alpha^2) \quad (42)$$

with  $\kappa_0(0) = 185$  MeV,  $a = 2.027$  and  $\rho_0(0) = 0.289$  fm<sup>-3</sup>,  $b = 1.115$ . In table 4 we give the  $\kappa_0$  values obtained from the ring calculation. Our  $\kappa_0$  values also seem to obey a parabolic dependence on  $\alpha$  but with  $a = 1.21$  and  $\kappa_0(0) = 112$  MeV. We may note here that the values of  $\kappa_0(0)$  and  $a$  in Ref. (14) were obtained by means of a least square polynomial fit to the BHF values of the binding energy and the values are quite sensitive to the degree of the polynomial used for the fit.

Our value of  $\kappa_0(0) = 112$  MeV is in good agreement with the one suggested by Brown and Osnes<sup>28</sup> for symmetric nuclear matter. At  $\alpha = 0.33$  the value of  $\kappa_0$  from our fit is 97 MeV which is close to the empirical value of 90 MeV used by Baron, Cooperstein and Kahana<sup>8</sup> to get the maximum explosion energy in their hydrodynamical calculations. From their numerical investigation the authors of Ref. (8) concluded that the softening of the EOS plays a crucial role in generating prompt explosion for stars in the mass range of 12 – 15  $M_\odot$  (where  $M_\odot \sim 2 \times 10^{23}$  g is the sun's mass). This conclusion has been questioned by more refined calculations<sup>29,30,31</sup>. However, even in models where the direct explosion mechanism fails, a softer EOS is helpful to the shock. The decrease in incompressibility with increase in  $\alpha$  is quite intuitive when we consider that going from bound symmetric matter to unbound neutron matter, the minimum of the binding energy gradually disappears. Therefore from eq. (40) the nuclear incompressibility decreases and vanishes for a certain value of  $\alpha$ .

### Conclusion

In conclusion, a fully microscopic calculation has been done using the ring-diagram summation for the EOS of asymmetric nuclear matter. The numerical computation has been done with both the Paris<sup>19</sup> and the Bonn<sup>20</sup> potentials and the results are in satisfactory agreement with the empirical values. The model-space size is treated as a parameter. The inclusion of ring-diagrams increases the role of tensor forces and both the binding energy and the saturation density values are lower and closer to the empirical values than those obtained with previous calculations. The symmetry energy values also show an improvement. and is in better agreement with other independent calculations. The derived incompressibility exhibits a parabolic dependence on the asymmetry fraction, in qualitative agreement with the empirical asymmetry dependence used in the literature.

The ring diagram approach employs an infinite order summation of particle-particle hole-hole ring diagrams. The infinite order summation technique of Yang,Heyer and Kuo<sup>2</sup> is applicable to particle-hole ring diagrams as well. But these diagrams have not been included in nuclear matter calculations. There is reason to believe that the effect of

the particle-hole ring diagrams on binding energy calculations is not very appreciable and they are less important than the particle-particle ring diagrams. The lowest-order ring diagram is the pph diagram of first order in  $G^M$ . The second-order diagram may be taken as either pphh or ph and is second order in  $G^M$ . Thus the contribution to the ground state energy shift from the ph diagrams comes from the three vertex diagram which is third order in  $G^M$  (fig. 1(d)). Studies<sup>32,33,34</sup> have indicated that the particle-hole diagrams converge rapidly and they may not be important in nuclear matter binding energy calculations. This view is also supported by some Lipkin model calculations<sup>2</sup>.

As noted earlier, an interesting result of our ring calculation is the existence of saturation at  $\alpha = 0.8$  which is not present in the MBHF calculation. This behaviour would be of relevance in astrophysical systems which are essentially neutron rich. It would be interesting to study the neutron star properties with this method. To do that one needs to extend the present calculation to higher densities in a relativistic frame work.

The authors would like to thank Prof. G. E. Brown for his support and encouragement throughout the course of this work.

- 
- \* Electronic address: jaya@vbphysics.net.in
- <sup>1</sup> T. Coester, S. Cohen, B. Day and C.M. Vincent, Phys. Rev. **C 1** (1970) 769.
  - <sup>2</sup> S. D. Yang, J. Heyer and T. T. S. Kuo, Nucl. Phys. **A 448** (1986) 420.
  - <sup>3</sup> H. Q. Song, S. D. Yang and T. T. S. Kuo, Nucl. Phys. **A 462** (1987) 491.
  - <sup>4</sup> M. F. Jiang, T. T. S. Kuo and H. Müther, Phys. Rev. **C 38** (1988) 2408.
  - <sup>5</sup> M. F. Jiang, R. Machleidt and T. T. S. Kuo, Phys. Rev. **C 41** (1989) 2346.
  - <sup>6</sup> H. A. Bethe, Ann. Rev. Nucl. Sci. **21** (1971) 93.
  - <sup>7</sup> S. O. Bäckman, G. E. Brown and J. A. Niskanen, Phys. Rep. **124** (1985) 1.
  - <sup>8</sup> E. Baron, J. Cooperstein and S. Kahana, Phys. Rev. Lett. **55** (1985) 126.
  - <sup>9</sup> M. Brack, C. Guet and H. B. Hakansson, Phys. Rep. **123** (1985) 277.
  - <sup>10</sup> S. H. Kahana, Ann. Rev. Nucl. Part. Sci. **39**, (1989) 231.
  - <sup>11</sup> H. Jaqaman, A. Z. Mekjian and L. Zamick, Phys. Rev. **C 27** (1983) 2782.
  - <sup>12</sup> R. K. Su, S. D. Yang, G. L. Li and T. T. S. Kuo, Mod. Phys. Lett. **A 1** (1986) 71.
  - <sup>13</sup> H. Q. Song, G. D. Zheng and R. K. Su, J. Phys. **G 16** (1990) 1861.
  - <sup>14</sup> I. Bombaci and U. Lombardo, Phys. Rev. **C 44** (1991) 1892.
  - <sup>15</sup> I. Bombaci, T. T. S. Kuo and U. Lombardo, Phys. Rep. **242** (1994) 165.
  - <sup>16</sup> H. Q. Song, Z. X. Wang and T.T.S. Kuo, Phys. Rev. **C 46** (1992) 1788.
  - <sup>17</sup> J. Cugnon, P. Deneye and A. Lejeune, Z. Phys. **A 328** (1987) 409.
  - <sup>18</sup> R. B. Wiringa, V. Fiks and A. Fabrocini, Phys. Rev. **C 38** (1988) 1010.
  - <sup>19</sup> M. Lacombe, B. Loiseau, J.M. Richard, R. Vinh Mau, J. Côte, P. Pires and R. de Tourreil, Phys. Rev. **C 21** (1980) 861.
  - <sup>20</sup> R. Machleidt, K. Hollinde and Ch. Elster, Phys. Rep. **149** (1987) 1.
  - <sup>21</sup> Z. Y. Ma and T. T. S. Kuo, Phys. Lett. **B 127** (1983) 137.
  - <sup>22</sup> T. T. S. Kuo and Z. Y. Ma, Nucleon-Nucleon Interaction and Nuclear Many-body Problems, eds. S. S. Wu and T. T. S. Kuo (World Scientific, Singapore, 1984) p. 178.
  - <sup>23</sup> T. T. S. Kuo, Z. Y. Ma and R. Vinh Mau, Phys. Rev. **C 33** (1986) 717.
  - <sup>24</sup> H. A. Bethe, Ann. Rev. Nuc. Sci. **21** (1971) 93.
  - <sup>25</sup> D. W. L. Sprung, Adv. Nucl. Phys. **5** (1972) 225.
  - <sup>26</sup> E. Schiller, H. Muether, P. Czerski, Phys. Rev. **C 59** (1999) 2934.
  - <sup>27</sup> O. Sjöberg, Nucl. Phys. **A 222** (1974) 161.
  - <sup>28</sup> G. E. Brown and E. Osnes, Phys. Lett **B 159** (1985) 223.
  - <sup>29</sup> S. W. Bruenn, Astrophys. J. (Suppl.) **58** (1985) 771.
  - <sup>30</sup> E. S. Myra and S. A. Bludman, Astrophys. J. **340** (1989) 384.
  - <sup>31</sup> E. Baron and J. Cooperstein, Astrophys. J. **353** (1990) 597.
  - <sup>32</sup> W. H. Dickhoff, A. Faessler, H. Muether, Nuc. Phys. **A 389** (1982) 492.
  - <sup>33</sup> H. Muether, NN interactions and the nuclear many-body problem, ed. S. S. Wu, T. T. S. Kuo, pg 490.
  - <sup>34</sup> B. D. Day, Phys. Rev. **C 24** (1981) 1203.